

Analysis and characterization of tin-doped ZnO nanostructures

M. Hermann¹, F. Bansil¹, H.A. Hunter^{2,*}

¹Institute of Energy, Jülich Research Centre, 52428 Jülich, Germany

²School of Physics, Purdue University, IN 47907, USA

*) E-mail: hah@purdue.edu



Received 15/5/2020, Accepted 21/9/2020, Published 15/5/2021

In this paper, undoped and tin-doped ZnO nanostructures were grown onto non-conductive substrates by a simple solution method. Structural, morphological, optical and electrical properties of the structures were investigated with respect to tin concentration. From XRD studies, all the ZnO nanostructures were found as hexagonal wurtzite type structures growing preponderantly oriented with *c*-axis normal to the substrate. An increase in tin content resulted in a decrease in grain size, whereas the dislocation density increases. SEM observations indicated that all the structures were textured throughout the substrates without any cracks or pores. The influence of incorporation of tin on surface morphology of the samples was clearly seen. Average diameter of the nanostructures decreased with increasing tin content. Absorption spectra of the structures revealed that the band gap of the films increases with increasing tin concentration. It is found that the tin-doped samples have higher average transmittance than the undoped one. The 1 % tin-doped sample exhibited ~80 % average transparency, which was the best transparency among the doped samples. Electrical measurements showed that resistivity of the structures increased with increasing dopant concentration. This increasing was attributed due to a decrease in carrier concentration caused by carrier traps at the grain boundaries.

Keywords: Sn; ZnO; Nanostructure.

1. INTRODUCTION

Transparent conducting films typically are made up of a layer of transparent conducting oxide (TCO), generally in the form of indium tin oxide (ITO), fluorine-doped tin oxide (FTO) and doped zinc oxide (ZnO) [1]. ZnO is a useful, economic and environmental material because of its typical properties such as wide direct band gap (~ 3.3 eV), large exciton binding energy (60 meV), and transparency in the visible range, non-toxicity, abundancy in nature etc. [2–4]. As a II–IV binary semiconductor, ZnO nanostructures have attracted considerable attention because of their good optical, electrical and easily tunable morphological properties and their potential applications in solar cells, solar energy–hydrogen conversion devices, photo electrochemical

(PEC) hydrogen generation applications and sensors [5–8]. The development of selective sensors is based on the use of ZnO nanostructures doped with different impurities such as Sn, Fe, Cu, Al, etc. [9]. Many dopants such as groups I and V and rare-earth elements have been used. Among those materials, tin can easily replace Zn ($r^{2+} = 0.074$ nm). Due to a decrease in carrier concentration caused by carrier traps at the grain boundaries, the resistivity and band gap of doped films increase with increasing dopant concentration [10]. Tin-doped ZnO structures obtained by different methods such as Successive Ionic Layer Adsorption and Reaction (SILAR), spray pyrolysis and sol–gel methods have been reported [9, 11, 12]. However, there is no study about tin-doped ZnO films derived by the chemical bath deposition (CBD) method. We think that the effects of tin doping on properties of ZnO nanostructures grown by using solution growth methods must be studied in detail. The CBD method is a promising, simple and effective technique because it is not necessary to feed power to the conductive substrates, as in electrochemical deposition, or carry out the process in pressure vessels, as in hydrothermal synthesis. By the CBD method a variety of nanostructures can be obtained simply by changing precursor chemicals, concentration of solution, growth temperature and growth time [3, 13]. In this work, the effects of tin doping on properties of ZnO nanostructures obtained by the CBD method have been investigated. With increasing doping concentration, changes in structure, morphology, optical properties and activation energies of conductivity were investigated in detail.

2. EXPERIMENTAL PROCEDURE

Undoped and Sn-doped ZnO films were prepared by a simple solution method, namely the CBD method. The non-conductive substrates used in the present study were microscope glass slides. Before the deposition, the substrates were cleaned as reported elsewhere [14]. After these treatments, the substrates exhibit good hydrophilic property [13], which is vitally important to obtain textured structures. 0.1 M $\text{Zn}(\text{NO}_3)_2 \cdot 6\text{H}_2\text{O}$ was dissolved in distilled water and the pH value of the zinc nitrate solution was adjusted to ~ 10 by adding aqueous ammonia. $\text{SnCl}_2 \cdot 2\text{H}_2\text{O}$ was added to the starting solutions as dopant source at the concentrations of 0, 1, 3 and 5 at.%. Each complex solution was stirred for 20 min. Then, the previously cleaned glass substrates were immersed and the solutions were heated to 90 °C. Heating rate was about 7 °C/min. Substrates were taken out from the bath after 20 min. The samples were exposed to a heat-treatment process at 640 K for 2 h to remove included hydroxide phase, if any. Structural analysis was carried out by using a Philips X'pert Pro X-ray diffractometer (XRD) with Cu $K\alpha$ radiation ($\lambda = 1.5418$ Å) at operating voltage and current of 40 keV and 35 mA, respectively. Surface morphology of each sample was observed using a scanning electron microscope (SEM, JEOL JSM-5500LV, Japan). Optical absorption spectra in the UV–Vis spectral range (200–1100 nm) of the structures were determined by using a UV–visible spectrophotometer (Hitachi U-1900). Current–temperature characteristics of the structures were investigated by a two-point-probe method in the temperature range of 300–523 K by using a Keithley 6487 interfaced with a computer by a home-made Labview program. The resistivity values of the structures were measured at room temperature by a four-probe method. Intervals between the probes were 1 mm.

3. RESULTS AND DISCUSSION

3.1 X-ray analysis

X-ray diffraction patterns of undoped and tin-doped ZnO nanostructures are presented in Fig. 1. It can be seen that from the figure, two strong diffraction peaks corresponding to (002) and (101) orientations are present and they are well indexed to hexagonal phase crystalline ZnO (wurtzite structure, space group: P63mc (186); $a = 0.3249$ nm, $c = 0.5206$ nm) and the data are in accordance with the JCPDS 36-1451 card.

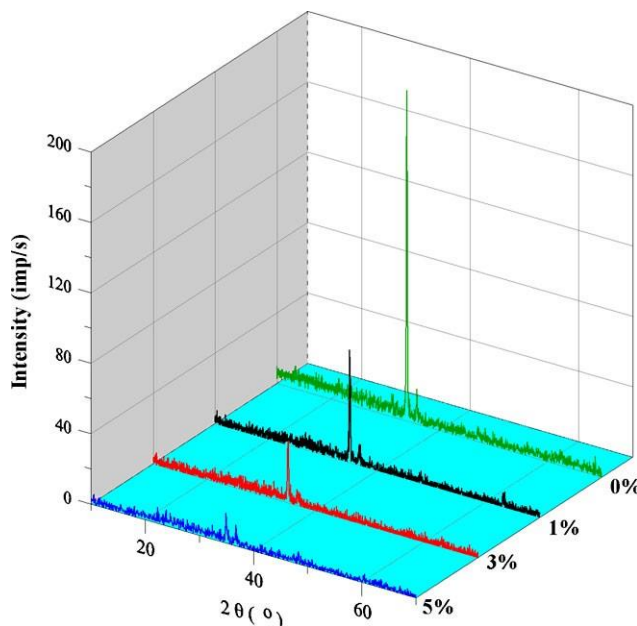


Fig. 1 X-ray diffraction patterns of undoped and tin-doped ZnO nanostructures

The greater intensities of (002) peaks in respective patterns indicate that crystallites grow preponderantly oriented with c -axis normal to the substrate. This preferential growing feature is correlated with the self-ordering effect determined by the film's trend to lower its surface energy during growth [15–17]. As is shown in [16] the film grains, after their coalescence, grow mainly in the direction normal to the substrate surface. In the case of hexagonal crystalline structure, this direction will be the [002] one, because this is the most closely packed and with the lowest free surface energy in the (002) plane, which will favor the grain growth in this direction. The intensity ratio of the (002) and (101) orientations was calculated as 14.23, 7.70, 6.5 and 1.8 for undoped, 1 %, 3 % and 5 % tin-doped ZnO nanostructures, respectively. This shows that preferential orientation of the structures is degenerated with respect to increasing tin concentration.

Table 1 The calculated average crystallite size (D), lattice spacing (d), full width at half maximum (FWHM) and diffraction angle of the nanostructures

	D	d (Å)	FWH	2θ (°)
Undo	47	2.637	0.1855	34.71

1 %	43	2.571	0.2016	34.87
3 %	33	2.568	0.2608	34.95
5 %	32	2.568	0.2742	34.91

diffractometer is broadened due to instrumental and physical factors (crystallite size and lattice strain) [19]. The calculated average crystallite size (D), lattice spacing (d), full width at half maximum (FWHM) and angle of diffraction of the films are given in Table 1. As seen from the table, average crystallite sizes of the films decrease with increasing tin concentration, whereas the (002) peak position shifts to higher diffraction angles. Decreasing in crystallite size is correlated by broadening of the XRD patterns, as indicated by corresponding increase in the FWHM values. In Bragg's formula ($2d \sin \theta = n\lambda$), it results that an increase of the interplanar spacing, as consequence of the lattice strain which may be induced in the structure during the preparation procedure by various factors such as impurities, lattice defects, vacancies or deformation faults, implies a shift to lower Bragg angle [20]. Jeong et al. [21] reported Al-doped ZnO thin films prepared by a spray pyrolysis method on glass substrates. They investigated the effects of Al doping on optical, electrical and structural properties of the ZnO films. They observed that the position of the peak (002) shifted to higher angles. They attributed this shift to residual stress in the film caused by the difference in ionic sizes between Zn^{2+} and Al^{3+} . In our study, we attributed that the shift of the position of the diffraction peak (002) to slightly higher angles result from the difference in ionic sizes between Zn^{2+} and Sn^{4+} . The dislocation density (δ), defined as the length of dislocation lines per unit volume of the crystal, can be estimated from the following relation using the simple approach of Williamson and Smallman [22]:

$$\delta = \frac{1}{D^2} \quad (1)$$

Average crystallite sizes and dislocation densities of the tin-doped ZnO films as a function of tin concentration are shown in Fig. 2. Results presented in Fig. 2 show that the dislocation density of the films increases with the concentration of tin in the starting solutions. Ilıcan et al. [23] reported tin-doped ZnO thin films derived by a sol-gel spin-coating method on glass substrates. They investigated the effect of tin dopant on the properties of the ZnO films. They reported that the dislocation density of the films increased with tin concentration. In our case, it can be attributed that this increasing in dislocation density of the films directly originates from the different ionic radii of Zn^{2+} and Sn^{4+} .

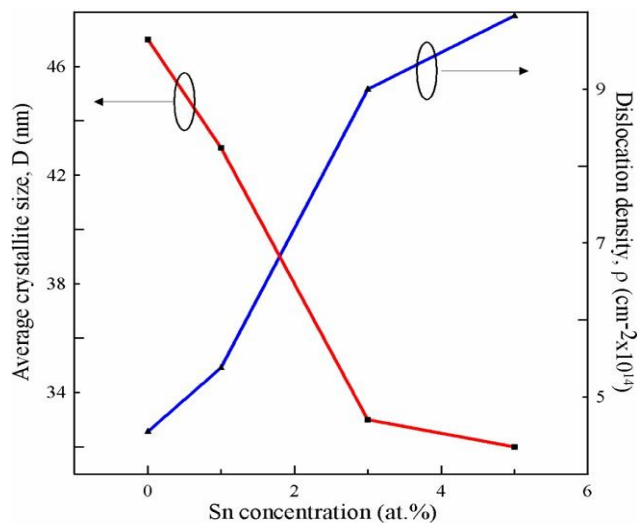


Fig. 2 Average crystallite sizes and dislocation densities of the tin-doped ZnO nanostructures as a function of tin concentration

3.2 Surface morphology

Figure 3 shows the SEM images of undoped and tin-doped ZnO nanostructures annealed in air for 2 h. It can be seen from the SEM images that all the structures were textured throughout the substrates without any cracks or pores and the morphology of the structures was affected from tin incorporation. The hexagonal shape of the nanostructures proves that rod-like nanostructures grew successfully on non-conductive substrates without using templates. Furthermore, the influence of incorporation of tin on surface morphology of the samples can be clearly seen. Average diameters of the structures were measured as 390, 280, 200 and 120 nm, which are corresponding to the tin-doped ZnO thin films with the concentrations of 0, 1.0, 3.0, and 5.0 at.%, respectively. It is clearly seen that with increasing tin doping concentration, average diameters of the structures decrease, which directly influences the sensitivity of a thin-film sensor. These SEM images reveal that morphology and size of the ZnO nanostructures could be tuned by adjusting tin dopant concentration and the results agree with XRD crystallite size calculations.

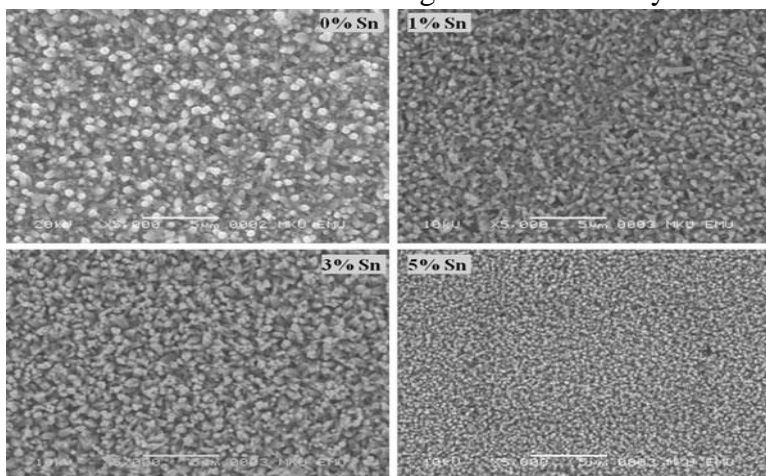


Fig. 3 SEM images of undoped and tin-doped ZnO nanostructures annealed in air for 2 h

3.3 Optical properties

Optical absorption spectra in the UV–Vis spectral range (200–1100 nm) of the structures were determined using a UV–visible spectrophotometer (Hitachi U-1900). The analysis of the dependence of absorption coefficient on photon energy in the high-absorption regions is performed to obtain the detailed information about the energy band gaps of the structures. The optical band gap of the structures is determined by the following relation [23]:

$$\alpha h\nu = B(h\nu - E_g)^m, \quad (2)$$

where B is an energy-independent constant, E_g is the optical band gap energy and m is an index that characterizes the optical absorption process and is theoretically equal to 2 and $1/2$ for indirect and direct allowed transitions, respectively. According to theoretical and practical results, ZnO exhibits direct interband transitions [24]. Thus, we can choose m as $1/2$. Plotting the graph of $(\alpha h\nu)^2$ against photon energy, $h\nu$, the band-gap value can be determined by extrapolating the straight-line portion. The cause of decreasing of the band gap after heat treatment is removal of the hydroxide phase from the film [25] and/or removal of defect levels, which is a more common phenomenon in chemically deposited thin films [26, 27]. Figure 4 shows the plots of optical transmittance spectra of the tin-doped ZnO nanostructures prepared on glass substrates by the CBD method and heat treated at 640 K for 2 h in air. It can be seen from the figure that the tin-doped samples have higher average transmittance than the undoped one. In our case, the 1 % tin-doped sample exhibited $\sim 80\%$ average transparency, which was the best transparency among the doped samples. The E_g values of undoped and Sn-doped ZnO nanostructures were determined as 3.16, 3.33, 4.06 and 4.13 eV, which are corresponding to the tin-doped ZnO nanostructures with the concentrations of 0, 1.0, 3.0 and 5.0 at.%, respectively (inset of Fig. 4). It is seen that the E_g values of the structures increase with increasing tin doping concentration. Tsay et al. [12] reported tin-doped ZnO thin films prepared by a sol–gel method on glass substrates. They investigated the effects of tin doping on the properties of the ZnO films. They observed that all samples show sharp absorption edges which were shifted to shorter wavelengths (blue shift) and band-gap energies of the films increased with increasing tin concentration.

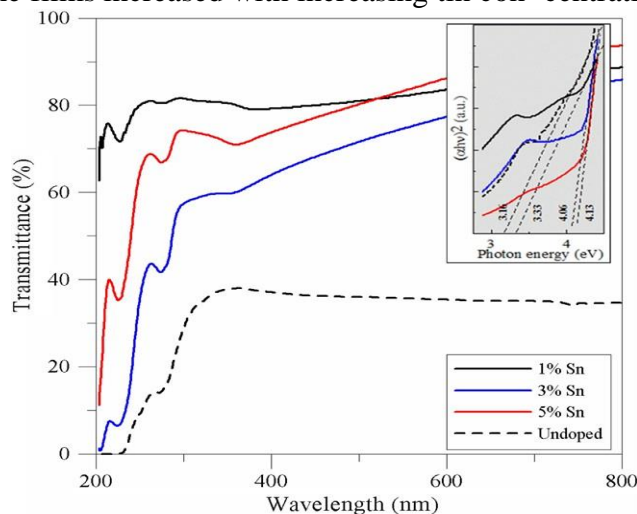


Fig. 4 Optical transmittance spectra of undoped and tin-doped ZnO nanostructures (*inset*: plots of $(\alpha h\nu)^2$ vs. photon energy, $h\nu$, of the structures)

They attributed this blue shift to the poor crystallinity of the ZnO films. As supported with XRD results, in our case, widening of band gaps of the structures can be related to the deterioration of crystallinity.

3.4 Electrical properties

The current–voltage (I – V) measurements of the samples have been carried out by a two-point-probe method in the temperature range of 300–523 K by using a Keithley 6487 interfaced with a computer by a Labview program. Silver electrodes were painted on deposited ZnO nanostructures to achieve ohmic contact with them. The derivative $(\partial I / \partial V)^{-1}$ is constant and practically equal to the dark electrical resistance of the investigated structures, indicating a negligible value of the contact resistance [28, 29]. Generally, ZnO films without any additional doping exhibit an n-type conduction due to the intrinsic defects, which are attributed to native defects such as the Zn interstitial atoms and the oxygen vacancies [30]. By using the thermal electromagnetic force (emf) method, n-type conductivity of the structures was also proved. To activate the electrical conductivity in an n-type semiconductor it is known that donor levels must be ionized with at least a minimum energy equal to the energy difference $E_C - E_D$, where E_C represents the valence band minimum and E_D the donor levels [31]. For ZnO films which have deeper levels (trap levels) (E_t), below the conduction band (E_C), the electrical conductivity depends on free carrier concentration (n) as in the equation below [32]. The N_C is a function of doping level, E_C is the density of states in the conduction band, E_t is the trap density and grain size, k is the Boltzmann constant and T is the absolute temperature. In the case of the temperature-activated mobility not being a dominant process [33], Eq. (4) can be used to calculate activation energy of the electrical conductivity. Due to the current passed through the film being proportional to free carrier concentration, the current–temperature plot ($\ln I - 1/T$) can be used to deduce the E_a/k value, from which the activation energy (E_a) of electronic transport for semiconducting materials can be calculated. The dependences of $\ln I$ on $1/T$ in the temperature range of 300–523 K for the tin-doped ZnO nanostructures is shown in Fig. 5. As seen from the figure, there are two linear regions. By using the slopes of the linear regions, the activation energies were calculated as 1.18, 0.41 eV; 0.48, 0.58 eV and 0.42, 0.23 eV, which are corresponding to the tin-doped ZnO nanostructures with the concentrations of 1.0, 3.0 and 5.0 at.%, respectively. Comparable values have been obtained in studies of polycrystalline ZnO [34, 35]. The $\ln I$ vs. $1/T$ curves exhibit humps at around 400 K at which the structures show metallic behavior (encircled parts in the figure). This critical behavior is commonly observed in magnetic semiconductors and known to be due to the scattering of carriers by magnetic spin fluctuations via exchange interaction [36]. The electrical characteristics of ZnO structures can be controlled by doping with ternary elements or by adjusting process conditions [12]. The resistivity values of the structures were measured at room temperature by a four-probe method. The results show that the undoped ZnO sample exhibits a resistivity of $1.5 \times 10^3 \Omega \text{ cm}$ and the

resistivity values of the 1, 3 and 5 at.% tin-doped ZnO samples were, 4.1×10^3 , 7.4×10^3 and $9.8 \times 10^3 \text{ } \Omega \text{ cm}$. The resistivity of the structures increased with increasing dopant concentration, which may be due to a decrease in carrier concentration caused by carrier traps at the grain boundaries.

4. CONCLUSIONS

In this work, the effects of tin doping on properties of ZnO nanostructures obtained by the CBD method have been investigated. With increasing doping concentration, changes in structure, morphology, optical properties and activation energies of conductivity were investigated in detail. We can conclude that • From XRD studies, undoped and tin-doped ZnO nanostructures were found as hexagonal wurtzite type structures growing preponderantly oriented with *c*-axis normal to the substrate. An increase in tin content resulted in a decrease in grain size, whereas the dislocation density increases.

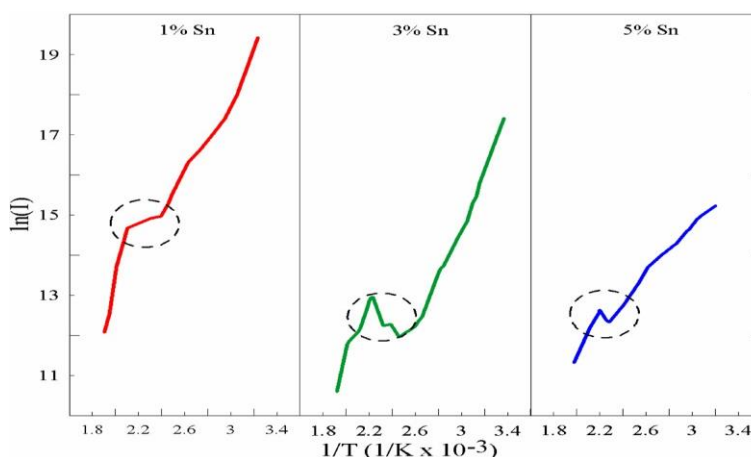


Fig. 5 Dependences of $\ln I$ on $1/T$ in the temperature range of 300–523 K for the tin-doped ZnO nanostructure.

According to SEM analysis, all the structures were texture throughout the substrates without any cracks or pores. The influence of incorporation of tin on surface morphology of the samples was clearly seen. Average diameter of the nanostructures decreased with increasing tin content. Optical absorption spectra in the UV–Vis spectral range of the films revealed that E_g values of the films increase with increasing Sn doping concentration. It is found that tin-doped samples have higher average transmittance than the undoped one. The 1 % tin-doped sample exhibited ~80 % average transparency, which was the best transparency among the doped samples. Electrical measurements show that the resistivity values of the structures increased with increasing dopant concentration. This increasing is attributed due to a decrease in carrier concentration caused by carrier traps at the grain boundaries.

References

- [1] M. Tadatsugu, *Semicond. Sci. Technol.* 20, (2005) 35
- [2] Y. Yan, L. Zhou, J. Zou, Y. Zang, *Appl. Phys. A, Mater. Sci. Process.* 94, (2009) 559
- [3] F. Bayansal, S. Kahraman, G. Çankaya, H.A. Çetinkara, H.S. Güder, H.M. Çakmak, *J. Alloys Compd.* 509, (2011) 2094
- [4] W. Bai, K. Yu, Q. Zhang, Y. Huang, Q. Wang, Z. Zhu, N. Dai, Y. Sun, *Appl. Phys. A, Mater. Sci. Process.* 87, (2007) 755
- [5] M. Antoine, H. Herman, *Exp. Theo. NANOTECHNOLOGY 4 (2020) 1*
- [6] F. Favier, E.C. Walter, M.P. Zach, T. Benter, R.M. Penner, *Science* 293, (2001) 2227
- [7] M. Seol, H. Kim, W. Kim, K. Yong, *Electrochem. Commun.* 12, (2010) 1416
- [8] N.H. Al-Hardan, M.J. Abdullah, A. Abdul Aziz, *Int. J. Hydrog. Energy* 35, (2010) 4428
- [9] S.T. Shishiyanu, T.S. Shishiyanu, O.I. Lupan, *Sens. Actuators B* 107, (2005) 379
- [10] J.H. Lee, B.O. Park, *Thin Solid Films* 426, (2003) 94
- [11] C. Deke, E. P. Petrik, *Exp. Theo. NANOTECHNOLOGY 4 (2020) 219*
- [12] C.Y. Tsay, H.C. Cheng, Y.T. Tung, W.H. Tuan, C.K. Lin, *Thin Solid Films* 517, (2008) 1032
- [13] M. Fragala, Y. Aleeva, G. Malandrino, *Superlattices Microstruct.* 48, (2010) 408
- [14] F. Bayansal, H.A. Çetinkara, S. Kahraman, H.M. Çakmak, H.S. Güder, *Ceram. Int.* 38, (2012) 1859
- [15] Z.Q. Xu, H. Deng, Y. Li, Q.H. Guo, Y.R. Li, *Mater. Res. Bull.* 41, (2006) 354
- [16] R.J. Hong, K. Helming, X. Jiang, B. Szyszka, *Appl. Surf. Sci.* 226, (2004) 378
- [17] H. Deng, J.J. Russell, R.N. Lamb, B. Jiang, Y. Li, X.Y. Zhou, *Thin Solid Films* 458, (2004) 43
- [18] V. Pecharsky, P. Zavalij, *Fundamentals of Powder Diffraction and Structural Characterization of Materials* (Springer, New York, (2005)
- [19] A. Van Der Drift, *Philips Res. Rep.* 22, (1967) 267
- [20] A.A. Dakhel, F.Z. Henari, *Cryst. Res. Technol.* 38, (2003) 979
- [21] S.H. Jeong, B.N. Park, S.B. Lee, J.H. Boo, *Surf. Coat. Technol.* 201, (2007) 5318
- [22] T. Philip, J. Maruc, K. Claire, *Exp. Theo. NANOTECHNOLOGY 4 (2020) 231*
- [23] S. Ilcan, M. Çağ lar, Y. Çağ lar, *Appl. Surf. Sci.* 256, (2010) 7204
- [24] C.M. Muiva, T.S. Sathiaraj, K. Maabong, *Ceram. Int.* 37, (2011) 555
- [25] M.L. de la Olvera, A. Maldonado, R. Asomoza, M. Melendez Lira, *Sol. Energy Mater. Sol. Cells* 71, (2002) 61
- [26] V.R. Shinde, C.D. Lokhande, R.S. Mane, S. Han, *Appl. Surf. Sci.* 245, (2005) 407
- [27] G. Hodes, A.A. Yaro, F. Decker, P. Motisuke, *Phys. Rev. B* 36, (1987) 4215
- [28] S.M. Sze, *Semiconductor Devices, Physics and Technology* (Wiley, New York, (1985)
- [29] R. Dalven, *Introduction to Applied Solid State Physics* (Plenum Press, New York, (1990)
- [30] U. Ozgur, Y.I. Alivov, C. Liu, A. Teke, M.A. Reshchikov, S. Dogan, V. Avrutin, S.J. Cho, H. Morkoc, *J. Appl. Phys.* 98, (2005) 041301
- [31] A.E. Jimenez-Gonzalez, J.A. Soto Urueta, R. Suarez-Parra, *J. Cryst. Growth* 192, (1998) 430
- [32] S. Major, A. Banerjee, K.L. Chopra, *J. Mater. Res.* 1, (1986) 300
- [33] J.W. Orton, M.J. Powell, *Rep. Prog. Phys.* 43, 1263 (1980)
- [34] E. Hahn, *J. Appl. Phys.* 22, (1951) 855
- [35] J. Lee, J.H. Hwang, J. Mashek, T. Mason, A. Miller, R. Siegel, *J. Mater. Res.* 10, (1995)

Exp. Theo. NANOTECHNOLOGY 5 (2021) 13–22

2295

[36] V.R. Shinde, T.P. Gujar, C.D. Lokhande, R.S. Mane, S.H. Han, *Mater. Chem. Phys.* 96, (2006) 326